Brain mechanisms of self-control: A neurocognitive investigation of reward-based action control and error awareness

Harsay, H.A.

Publication date
2014

Appendix

Appendix Chapter 3

Supplemental Figure 1. (related to Figure 2) Reward anticipation> no reward anticipation: cue locked and sustained BOLD response

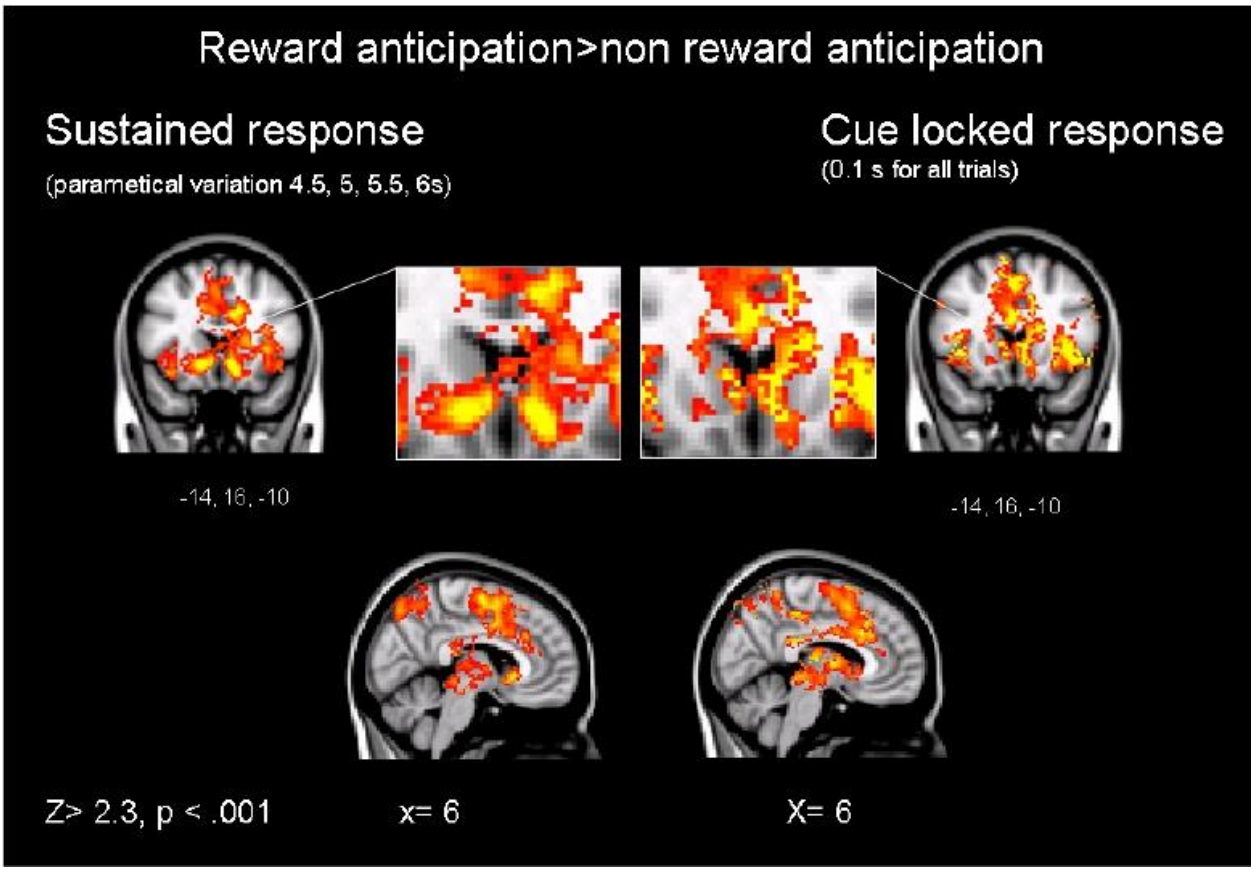

Figure caption Supplemental Figure 1. Anatomical localization of regions showing significant positive increase with sustained activation during the parametrically varied interval (4.5 seconds, 5 seconds, 5.5 seconds, 6 seconds from cue onset) and phasic cue locked activation (during 0.1 seconds from cue onset) between reward and non-reward trials. Little difference in the hemodynamic response is observed whether using a parametric sustained model, or a phasic cue-locked model (similar to the lack of interaction in the behavioral results). Renderings (on MNI stereotactic space) are thresholded at z>2.3.

Supplemental Figure 2 (related to Figure 2). Neural activation during specific oculomotor preparation.

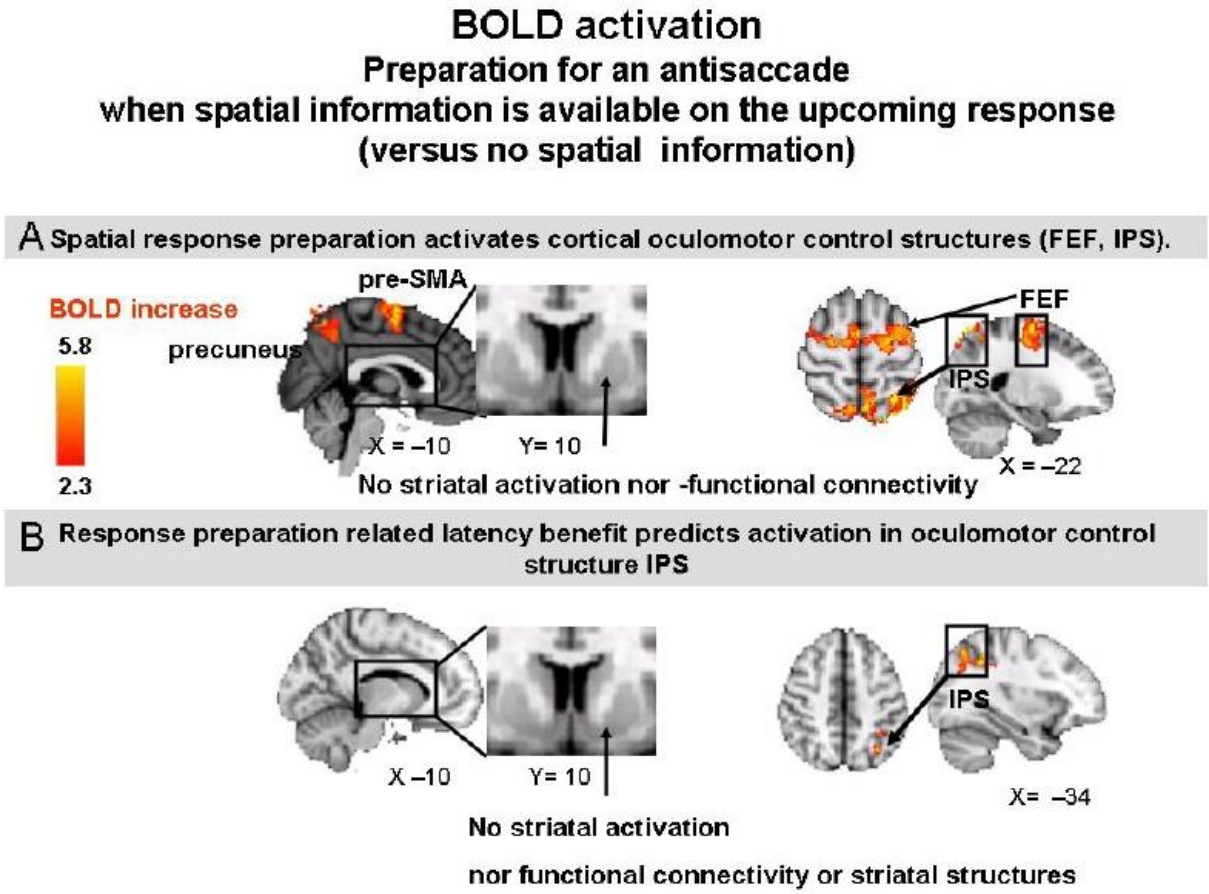

Figure caption Supplemental Figure 2.

A. Anatomical localization of regions showing significant positive increase with direction-specific (spatial) knowledge on the upcoming antisaccade. Renderings (on MNI stereotactic space) are thresholded at z,2.3. and Left: Saggital rendering (lateral view) showing activation clusters in oculomotor areas (presupplementary motor area (pre- SMA) and precuneus), but no activation in the striatum (coronal rendering (zoomed-in medial view) of basal ganglia). Right: Axial rendering (top view) and saggital rendering (lateral view) showing activation clusters in oculomotor areas frontal eye fields (FEF) and intraparietal sulcus (IPS). Striatum seeded functional connectivity analysis confirmed absence of striatal functional connectivity during direction-specific preparation. B. Anatomical localization of regions showing significant positive increase when antisaccade latency profits from direction-specific (spatial) knowledge on the upcoming antisaccade. Right: Axial rendering (top view) and saggital rendering (lateral view) showing activation clusters in oculomotor area intraparietal sulcus (IPS) and absence of striatal activation during direction-specific preparation, that was confirmed by analysis of striatal connectivity during direction-specific preparation as modulated by preparationrelated antisaccade benefits.

Supplemental Table 1 a. Brain regions showing significant functional activation during oculomotor preparation for an antisaccade when direction-specific information (versus direction-nonspecific information) on the upcoming antisaccade is available.

Brain region	X	Y	Z	Max z
R frontal eye fields	24	-12	64	4.49
L frontal eye fields	-22	-10	64	4.91
Supplementary motor area	4	-4	64	4.86
R intraparietal sulcus				
L intraparietal sulcus	-38	-56	56	5.11
Precuneus cortex	-4	-54	46	4.11
R middle temporal gyrus	62	-52	16	3.63
L middle temporal gyrus	-48 -	52	10	3.36
L superior lateral occipital cortex	-12	-82	54	3.67

Note: Local maxima of activation of all significant clusters (at z= 2.3, p= .05, clustercorrected) are displayed. All coordinates are given in MNI space.

Supplemental Table 1 b. Brain regions in which activation during direction-specific oculomotor preparation- versus direction-nonspecific oculomotor preparation, covaried with direction- specific preparation-related antisaccade latency benefit.

Brain region	X	Y	Z	Max z
L frontal eye fields	-30	-26	64	2.52
R intraparietal sulcus	4-	-68	44	2.4
Precuneus cortex	-6	-42	64	2.67
L GM visual cortex	8	-70	18	3.28
L lateral occipital cortex	38	-74	20	4.23

Note: Local maxima of activation of all significant clusters (at z= 2.3, p= .05, clustercorrected) are displayed. All coordinates are given in MNI space.

Supplemental Figure 3 (related to Figure 2). Reward anticipation and antisaccade accuracy.

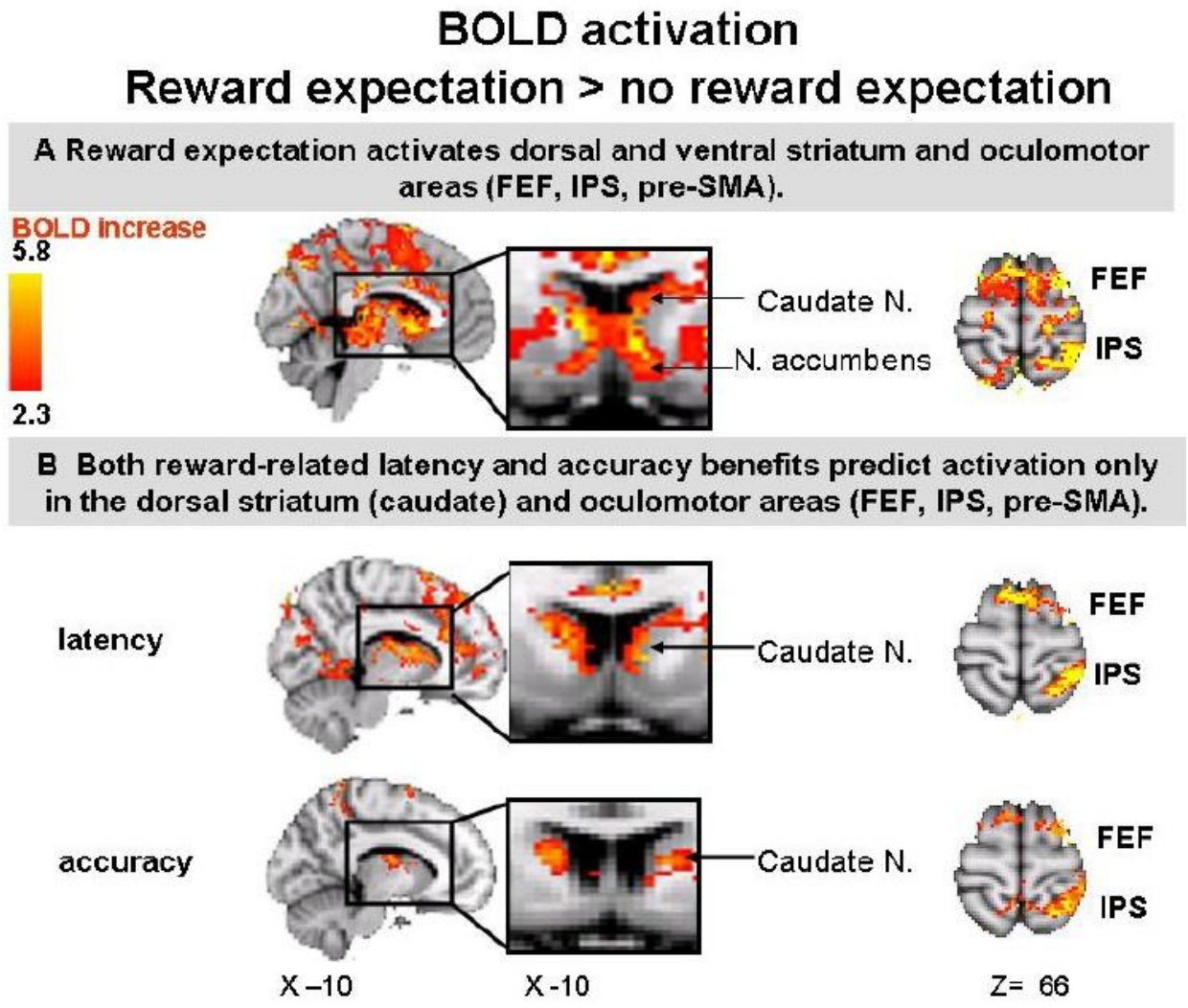

Figure caption Supplemental Figure 3. Reward anticipation and antisaccade accuracy. (A) Anatomical localization of regions showing significant positive increase when expecting reward for a well performed antisaccade. Renderings (on MNI stereotactic space) are thresholded at z,2.3.

(B). Anatomical localization of regions showing significant positive increase when antisaccade latency and accuracy profits from reward expectation. Reward-related latency and accuracy benefits show topographically similar patterns. Saggital rendering (lateral view) and coronal rendering (medial view) showing only dorsal striatum (caudate) clusters and oculomotor clusters (pre-supplementary motor area, precuneus, FEF, IPS)

Supplemental Figure 4 (related to methods)

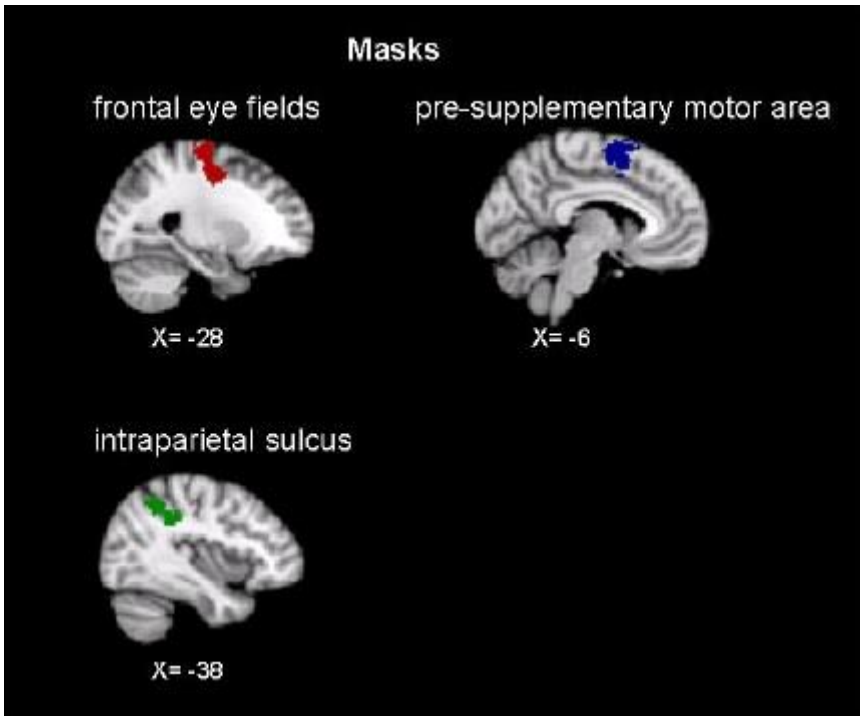

Figure caption Supplemental Figure 4. Masks.

Depicted are the masks for the quantification of the difference of the strength of the behaviorally modulated functional connectivity (caudate versus accumbens) with the cortical eye fields (frontal eye fields, intraparietal sulcus) and pre-supplementary motor area. The definition of the masks was based on a combination of functional and anatomical landmarks.

Appendix Chapter 4

S 1. Supplementary methods

S 1. 1. Participants. Mean estimated verbal IQ (NLV-IQ (Schmand et al., 1992); corrected for age and gender was 118.5 (SD 19.7) and mean non-verbal IQ according to the Raven Progressive Matrices part A and B (Raven, 1984) was 111.6 (SD 16.7). None of the participants obtained a score outside the normal range on neuropsychological tests administered in the screening: None of the participants had mild cognitive impairment as measured by the cognitive screening test (De Graaf & Deelman, 1991) or memory problems as assessed by the Digit span forward and backward (Wechsler, 1997) and the Revised Visual Retention Test [Benton, 1963]). Scores on the Test-d2 (Brickenkamp, 1962) and Stroop Color Word Test (Stroop, 1935) were in the normal range as well as scores on a standard health questionnaire (Symptom Check List-90-Revised [Derogatis, 1994]),

Multidimensional Fatigue Inventory [MFI-20 fatigue; Smets et al., 1995] and on a Subjective Well-being scale for Older Persons [Tempelman, 1987]). To verify that the elderly participants had no radiological signs of Alzheimer, we applied the standardized radiological procedure designed for patients suspected of having dementia. A qualified radiologist rated structural FLAIR and T1-weighted MRI-images of all participants to exclude brain abnormalities and incidental findings and second to systematically score for focal atrophy of medial temporal lobe and hippocampus and for vascular disease (i.e. infarcts, white matter lesions). The degree of medial temporal lobe atrophy including the hippocampal formation (the width of the choroid fissure, width of the temporal horn, and height of the hippocampal formation) and surrounding spaces occupied by cerebrospinal fluid was scored using the MTA-scale for Medial Temporal lobe Atrophy (Scheltens et al., 1992). White matter lesions and lacunes were scored with the Fazekas scale (Wahlund et al., 2001). None of the participants was in the pathological range on any of these integrity measures.

S 1. 2. Procedures. After a first telephone screening with a general intake procedure and with the administration of the cognitive screening test (De Graaf & Deelman, 1991) to exclude participants with signs of mild cognitive impairment, the experiment involved three test sessions: A neuropsychological- and health-screening session, a second behavioral task session outside the scanner (data are reported in Harsay et al., 2010) and a third task session inside the scanner, of which the eyetracking data and the independently acquired DTI (diffusion tensor imaging) and T1 structural (used for gray matter) data are reported here. During this third task session, participants were first presented a series of trials outside the scanner to familiarize themselves with the stimulus-reward associations and antisaccade response requirements. Participants then completed two 25-minute experimental blocks inside the scanner, each comprising 128 trials. The participants received a financial compensation of 71 Euro for participation. Depending on their performance on the reward trials of the antisaccade task, they could win a monetary reward of 12, 80 Euro per block.

S 1. 3. Eyetracking and stimulus delivery set-up. In the MRI scanner the participant's left eye was continuously monitored with an MRI-compatible infrared oculographic limbus tracker (www.mrivideo.com) attached to the head coil and placed 3 cm beneath the participant's left eye. Eye movements were recorded with ViewPoint Eyetracker PC-60 (Version 2.7, www.arringtonresearch.com) software on a standard PC. Bidirectional communication between this PC and a second one responsible for the delivery of stimuli (using Presentation software, www.neurobs.com) ensured that stimulus onset times were registered in the eye movement data and that adequate feedback was provided to oculomotor responses on each trial. Eye movements were registered with a sampling rate of 60 Hz along with signals marking the stimulus onset times. Before task onset a 9-point calibration procedure was performed. Calibration and stimuli were presented on a 66 cm x 88 cm screen, placed at a 4-m viewing distance at the front end of the scanner and seen through a mirror above the participants' heads. Light in the scanning environment was constrained to video presentation of stimuli against a black background. To eliminate slow

drift in eye tracking-signal during the task, calibrated eye position was manually corrected to the central fixation cross. Regions of interest were defined by two peripheral outer square outlines (the endpoints of the antisaccade eye movements) surrounding the central fixation dot. The PC which tracked eye movements, signaled to the stimulus presentation PC when an eye movement left the fixation region and entered one of the target regions. The Presentation PC recorded correct trials versus errors and presented feedback accordingly.

S 1. 4. Analysis. Saccade parameters were detected with in-house developed software implemented in Java 1.5 (www.java.com) using minimum amplitude (>1.5°) and velocity (>30°/s) criteria and were visually inspected and double-checked for accuracy. In line with common definitions (Fischer et al., 1993) saccades with a latency of less than 80 ms after the display of the peripheral antisaccade target were classified as anticipatory responses. Exclusion criteria applied to trials in which participants failed to focus their eyes on the central instruction cue, trials in which gaze was not at fixation 200 ms before target appearance, trials with blinks during saccadic execution and trials exceeding 800 ms (miss). A trial without a premature eye movement towards the peripheral antisaccade target and with a saccade landing at the location of the square outline on the opposite side of the screen executed within 800 ms was classified as a correct trial. Only correct trials (92.4% ± 1.6) were taken into account to estimate the mean saccadic onset latency, defined as the time required to initiate a saccade toward a target after its presentation (Dorris et al., 1997; Munoz et al., 2000; Munoz and Everling, 2004). Antisaccade latencies and accuracy were analyzed with a 2x2x4x2x2 within-participants ANOVA design with Bonferroni correction. One factor was reward expectation (two levels: reward versus no reward expected for a well performed saccade) and another factor was spatial response preparation (two levels: direction-specific cue versus direction-nonspecific cue). To control for interaction effects with reward expectation or spatial preparation, we added 3 factors to the analysis: 1) the delay between the cue and the target (four levels: 4.5s, 5s, 5.5s, 6 s), 2) cue direction (two levels: left, right) and run (two levels: first, second). In order to calculate peformance benefits, we computed the relative reaction time (RT) advantages as [(RTno reward anticipation – RTreward anticipation)/RTno reward anticipation] for all participants, in line with common definitions (Schott et al., 2007). Accordingly, we computed the behavioral benefit from spatial preparation as [(RTdirection-nonspecific prep – RTdirection-specific prep)/RTdirection-nonspecific prep]. To investigate the link between individual differences in behavioral benefits and striatal fibertracts, the individual performance benefits in antisaccade latency were orthogonalized with the group mean separately for each instruction cue type (reward versus non reward and direction-specific preparation versus direction-nonspecific preparation). These demeaned condition-related benefits for each subject were correlated with the probabilistic diffusion tractography data of the striatum (caudate, putamen, nucleus accumbens) and with fractional anisotropy (FA) values.

S 1. 5. Preprocessing and analysis of fractional anisotropy and tractography of DTIs

To prepare the DTI's for analysis of fractional anisotropy and tractography, the brain was skull-stripped and extracted based on the B0 image with BET (Smith, 2002). We corrected DTI's for eddy currents and possible head motion (Jenkinson and Smith, 2001) by affine registration to a reference volume. A tensor model was fitted to the raw diffusion data using

FMRIB's Diffusion Toolbox (Behrens et al., 2003a; Behrens et al., 2003b) to generate FA images. The two consecutively acquired DTI data sets were averaged together to improve signal-to-noise ratio.

S 1. 6. Fractional Anisotropy

To create a mean FA skeleton for all participants, we applied a nonlinear registration method with more degrees of freedom than an affine transformation to align the brain on the basis of white-matter tracts (vs the whole brain) which is of advantage when analyzing FA differences between participants as it avoids mismatches between participants. Furthermore, as the standard space commonly used to align participants data is based on young to middle aged adult's brains, the standard space image may not be representative for an aging population. Therefore, FA images were aligned with tract-based spatial statistics (TBSS) (Smith et al., 2006) to every other one to determine the most "typical" image of the sample to be used as the target image for alignment. Each subject's aligned FA data were then projected onto this skeleton. The resulting mean FA skeleton depicts the centers of all tracts common to the group. For the reporting of standard space coordinates, the target image (i.e. the "most typical sample brain") was affine-aligned into MNI152 standard space and every image was transformed into 1x1x1mmMNI152 space by combining the nonlinear transform to the target FA image with the affine transform from that target to MNI152 space. The degree of FA has been related to properties of the tissue such as fiber diameter and fiber tract coherence, myelination and other characteristics of white matter. A larger FA value denotes a distortion of Brownian motion, which signifies the presence of coherent white matter tracts. Values closer to 0 indicate more isotropic diffusion of water molecules (showing Brownian motion), and absence or little coherence of white matter tracts. To locate white matter fibers that predict performance benefits we computed correlations between fractional anisotropy values in each voxel of the brain and individual differences in antisaccade performance benefit across participants. Thus, at each voxel, we correlated FA values with the antisaccadic benefit from reward anticipation [(RTno reward anticipation – RTreward anticipation)/RTno reward anticipation] and with the antisaccadic benefit from spatial preparation [(RTdirection-nonspecific prep – RTdirection-specific prep)/RTdirection-nonspecific prep]. For this purpose, the preprocessed data were fed into voxel-wise cross-subject statistics to determine significant voxels that varied with reward-related antisaccade performance benefits. This was done with an FSL-based randomisation program that performed permutation testing with 10.000 iterations. We considered differences in FA value significant at a cluster-based threshold with a p-value of 0.05 corrected for multiple comparisons (bonferroni). This resulted in the localisation of the parts of the white matter that predicted higher fractional anisotropy values with a higher benefit from reward anticipation (across participants).

S 1. 7. Tractography. All tractography was done in each participant's native space (nonnormalized) data, and resulting maps were warped into the most "typical" image of the elderly sample. For reporting coordinates, this representative group image was affine-aligned into MNI152 standard space. Every image was transformed into 1x1x1mmMNI152 space by combining the nonlinear transform to the target image with the affine transform from that target to MNI152 space. Probabilistic Tractography has been used to estimated multiple fiber

orientation within each voxels as crossing-fiber approaches yield more reliable results compared with single-fiber models. Thus we determined the number of crossing fibers per voxel using FSL- BEDPOSTX (Bayesian Estimation of Diffusion Parameters Obtained using Sampling Techniques (Behrens et al., 2007). BEDPOSTX estimated diffusion parameters by Markov Chain Monte Carlo sampling to build up distributions on the diffusion parameters (diffusion tensor, eigenvector and eigenvalue) at each voxel. By estimating spatial probability distributions, probabilistic tractography accounts for uncertainty inherent in local fiber directions (Behrens et al., 2003b). The resulting eigenvector with the largest value represents the principal water diffusion direction. For the estimation of tract strength between the basal ganglia and cortical areas, six separate seed structures were manually segmented: caudate, putamen and nucleus accumbens, for each hemisphere separately. In order to achieve anatomical precision in the labelling of individual seed structures, basal ganglia structures were defined individually per participant based on individual anatomical landmarks in the acquired individual DTI, B0 and T1 images (Jones and Cercignani, 2010) in combination with anatomical landmarks derived form published three-dimensional probabilistic cytoarchitectonic maps in the MNI structural atlas of the FSL Atlas Toolbox and checked by two raters (Eickhoff et al., 2007; Mazziotta et al., 1995). All analyses were done separately for each hemisphere.

S 1. 8. Individual differences analyses of probabilistic tractography

Due to inter-subject variability in the spatial distribution of the fibertracts, only voxels were included in the analyses for which at least ten participants had non-zero tract estimates. Next, voxel values were converted into proportions, such that the value at each voxel becomes the number of samples reaching the target mask for that image, divided by the number of samples that reach any target mask. The resulting brain image displayed a value for each voxel (though generally many of these are zero) representing the connectivity value between that voxel and the voxels in the basal ganglia seed region (number of fibers that pass through that voxel) that varied with the level of performance benefit. To identify significant regions, we used a cluster corrected threshold of $p < .01$ with at least 20 contiguous voxels.

S 2. Supplementary results

S 2. 1. Overal antisaccade performance

Mean onset latency and accuracy of antisaccades was 370 ms ± 11 (SE) and 92.4% ± 1.6. Antisaccade latency decreased in a linear fashion with the delay length between cue and target: the more time available to prepare the antisaccade, the shorter the antisaccade latency (from a mean latency of 386 ms ± 10 (SD) in the shortest delay down to 355 ms ± 11 (SE) in the longest delay, $F(3,45) = 21.153$, $p < .001$), suggesting that participants used the delay between cue and target for antisaccade preparation.

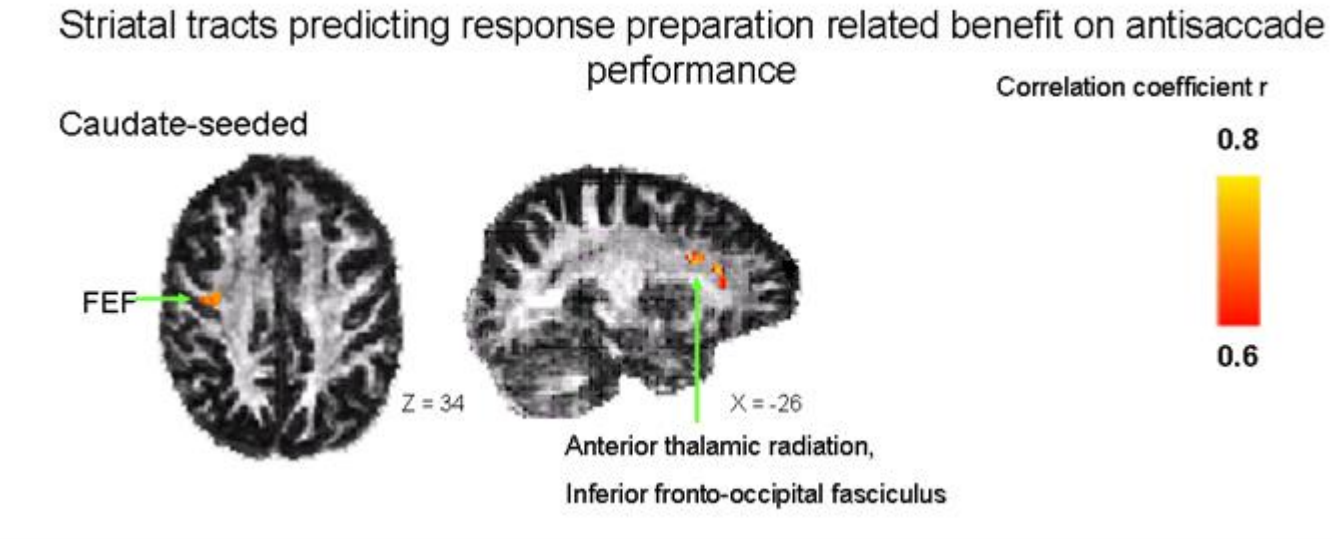

S Figure 2. 2. Fiber tracts from the striatum as associated with the effect of spatially specific oculomotor preparation cues on the latency of antisaccades, plotted on the most typical brain within our sample of older adults. Participants who speed up their antisaccades more than others when they have a priori knowledge on the direction of the upcoming antisaccade, show stronger fiber tracts between the caudate and the frontal eye fields and between the caudate and the anterior thalamic radiation. From left to right: Axial rendering (top view) showing clusters in the frontal eye fields; sagittal rendering (lateral view) showing clusters in white matter tracts anterior thalamic radiation and fronto-occipital fasciculus. Note FEF= frontal eye fields.

S 2. 3. Fractional anisotropy as associated with the effect of motivational incentives on the latency of antisaccades. Analysis of white matter density (FA) confirmed that performance improvements based on reward anticipation correlated with higher FA in the caudate, nucleus accumbens, thalamus, FEF, IFG, and frontopolar/orbitofrontal cortex (all Z-scores > 3.5, $p<0.0001$, Table 4). Performance improvements based on spatially specific oculomotor preparation, on the other hand, correlated with FA values in the supplementary motor cortex, the frontal medial cortex and areas in the occipital cortex, but not the ventral striatum (nucleus accumbens).

	X, Y, Z	Max z
Reward benefit		
R Accumbens	11, 20, -11	5.5
R Caudate	12, 17, 6	3.6
R Thalamus	20, -18, 16	6.1
L Frontal eye fields	-16, -2, 50	5.3
L Inferior Frontal gyrus	-49, 19, 17	4.4
L Frontopolar/Orbitofrontal cortex	-43, 38, -14	4.1
Oculomotor preparation benefit		
L Supplementary motor cortex	-11, 5, 47	4.6
R Frontal medial cortex	4, 40, -15	4.6
L Intracalcarine cortex	-16, -68, -11	5.2
R Lateral occipital cortex	43, -59, 45	5.6
L Lateral occipital cortex	-38, -74, -11	4.6

All Z-scores > 3.5 ($p<0.0001$)

S Table 2. 4. White matter density results. FA values as correlated with the effect of reward anticipation and spatially specific oculomotor preparation on the latency of antisaccades. Whereas a higher fractional anisotropy in both dorsal and ventral striatum, thalamus, frontal eye fields and inferior frontal gyrus is associated with benefit from reward expectation, fractional anisotropy in the supplementary motor cortex, the fronto-medial cortex and occipital areas, but not the striatum, is associated with benefit from specific oculomotor preparation.

References appendix Chapter 4

Behrens, T.E., Berg, H.J., Jbabdi, S., Rushworth, M.F., Woolrich, M.W., 2007. Probabilistic diffusion tractography with multiple fibre orientations: What can we gain? Neuroimage 34, 144-155.

Behrens, T.E., Johansen-Berg, H., Woolrich, M.W., Smith, S.M., Wheeler-Kingshott, C.A., Boulby, P.A., Barker, G.J., Sillery, E.L., Sheehan, K., Ciccarelli, O., Thompson, A.J., Brady, J.M., Matthews, P.M., 2003a. Non-invasive mapping of connections between human thalamus and cortex using diffusion imaging. Nat Neurosci 6, 750-757.

Behrens, T.E., Woolrich, M.W., Jenkinson, M., Johansen-Berg, H., Nunes, R.G., Clare, S., Matthews, P.M., Brady, J.M., Smith, S.M., 2003b. Characterization and propagation of uncertainty in diffusion-weighted MR imaging. Magn Reson Med 50, 1077-1088.

Brickenkamp, R. (1962). Aufmerksamkeits-Belastungs-Test. [The d2 test of Attention.] (1st ed.). Göttingen: Hogrefe.

De Graaf , A., & Deelman, B. G. R. (1991). Cognitive Screening Test: Handleiding voor Afname en Scoring. Lisse: Swets & Zeitlinger B. V.

Derogatis, L.R. (1994).SCL-90-R: symptom checklist-90-R: administration, scoring and procedures. Manual (3rd ed.). Minneapolis: national computer systems. Psychopharmacology Bulletin, 9, 13-27

Dorris, M.C., Pare, M., Munoz, D.P., 1997. Neuronal activity in monkey superior colliculus related to the initiation of saccadic eye movements. J Neurosci 17, 8566-8579.

Eickhoff, S.B., Paus, T., Caspers, S., Grosbras, M.H., Evans, A.C., Zilles, K., Amunts, K., 2007. Assignment of functional activations to probabilistic cytoarchitectonic areas revisited. Neuroimage 36, 511-521.

Fischer, B., Weber, H., Biscaldi, M., 1993. The time of secondary saccades to primary targets. Exp Brain Res 97, 356-360.

Jenkinson, M., Smith, S., 2001. A global optimisation method for robust affine registration of brain images. Med Image Anal 5, 143-156.

Jones, D.K., Cercignani, M., Twenty-five pitfalls in the analysis of diffusion MRI data. NMR Biomed 23, 803-820.

Mazziotta, J.C., Toga, A.W., Evans, A., Fox, P., Lancaster, J., 1995. A probabilistic atlas of the human brain: theory and rationale for its development. The International Consortium for Brain Mapping (ICBM). Neuroimage 2, 89-101.

Munoz, D.P., Dorris, M.C., Pare, M., Everling, S., 2000. On your mark, get set: brainstem circuitry underlying saccadic initiation. Can J Physiol Pharmacol 78, 934-944.

Munoz, D.P., Everling, S., 2004. Look away: the anti-saccade task and the voluntary control of eye movement. Nat Rev Neurosci 5, 218-228.

Raven, J.C. (1984). Manual for the Coloured Progressive Matrices (Revised). Windsor, UK: NFERNelson.

Scheltens, P., Leys, D., Barkhof, F., Huglo, D., Weinstein, H.C., Vermersch, P., Kuiper, M., Steinling, M., Wolters, E.C., Valk, J., 1992. Atrophy of medial temporal lobes on MRI in "probable" Alzheimer's disease and normal ageing: diagnostic value and neuropsychological correlates. J Neurol Neurosurg Psychiatry 55, 967-972.

Schmand B, Lindeboom J, van Harskamp F: Dutch Adult Reading Test. Lisse, Swets en Zeitlinger, 1992.

Schott, B.H., Niehaus, L., Wittmann, B.C., Schutze, H., Seidenbecher, C.I., Heinze, H.J., Duzel, E., 2007. Ageing and early-stage Parkinson's disease affect separable neural mechanisms of mesolimbic reward processing. Brain 130, 2412-2424.

Smets, E.M.A., Garssen, B., Bonke, B. & Haes, de J.C.J.m. (1995). The Multidimensional Fatigue Inventory (MFI); Psychometric qualities of an instrument to asses fatigue. Journal of Psychosomatic Research, 39, 315-325.

Smith, S.M., 2002. Fast robust automated brain extraction. Hum Brain Mapp 17, 143-155.

Smith, S.M., Jenkinson, M., Johansen-Berg, H., Rueckert, D., Nichols, T.E., Mackay, C.E., Watkins, K.E., Ciccarelli, O., Cader, M.Z., Matthews, P.M., Behrens, T.E., 2006. Tract-based spatial statistics: voxelwise analysis of multi-subject diffusion data. Neuroimage 31, 1487-1505.

Stroop, J.R. (1935). Studies of interference in serial verbal reactions. Journal of Experimental Psychology, 28, 643-662.

Tempelman, C. J. J. (1987). Welbevinden bij ouderen: konstruktie van een meetinstrument (Well-being in the elderly: Development of the scale subjective wellbeing older persons). Dissertation, University of Groningen, Groningen, The Netherlands.

Wahlund, L.O., Barkhof, F., Fazekas, F., Bronge, L., Augustin, M., Sjogren, M., Wallin, A., Ader, H., Leys, D., Pantoni, L., Pasquier, F., Erkinjuntti, T., Scheltens, P., 2001. A new rating scale for age-related white matter changes applicable to MRI and CT. Stroke 32, 1318-1322.

Appendix Chapter 6

Table A1

Brain region	X	Y	Z	Max z
R anterior insula cortex	34	18	−12	3.65
R mid insula cortex	50	8	−4	3.63
R postcentral gyrus (somatosensory cortex BA2R)	54	−26	44	3.04
L postcentral gyrus (somatosensory cortex BA2L, BA1L, BA3bL)	−46	−28	50	4.86
R thalamus	10	−24	10	3.15
L thalamus	−8	−22	8	4.39
R brain stem	8	−30	−8	3.21
R rostral anterior cingulate cortex	2	26	16	3.18
L rostral anterior cingulate cortex	−2	26	16	3.18
R dorsal anterior cingulate cortex	4	20	36	3.03
L dorsal anterior cingulate cortex	−4	32	32	3.64
R supplementary motor cortex (BA6R)	6	8	56	3.63
L supplementary motor cortex (BA6L)	−6	6	60	3.04
R precuneus cortex	4	−68	42	3.08
R inferior frontal gyrus	52	12	20	3.06
L inferior frontal gyrus	−48	12	22	2.48
R frontal eyefields BA8R, BA6R	20	−4	70	3.63
L frontal eyefields BA8L, BAL	−28	−26	70	4.22
R anterior intraparietal sulcus	−50	−44	50	4.23
L anterior intraparietal sulcus	40	−48	50	3.63
R parietal occipital junction (superior parietal lobe/lateral occipital lobe)	36	−58	40	3.72
L parietal occipital junction (superior parietal lobe/lateral occipital lobe)	−32	−60	40	4.30

Aware errors > unaware errors, BOLD activation cluster-corrected at z = 2.3, p = 0.001. Coordinates are given in MNI space.

Table A1. Complete list of brain regions showing significant BOLD activation during aware errors as compared to unaware errors.

Table A2

Brain region	X	Y	Z	Max z
R anterior insula cortex	34	14	−4	2.94
L anterior insula cortex	−40	16	−6	2.94
L mid insula cortex	−40	−12	10	2.82
L postcentral gyrus	−42	−34	50	3.09
R thalamus	14	−22	8	3.39
L thalamus	−10	−22	8	2.91
R brain stem	10	−22	−12	2.80
Supplementary motor area	2	−12	64	2.85
Dorsal anterior cingulate cortex	2	8	44	3.28
Supplementary motor area	2	−12	64	2.85
Precuneus cortex	2	−64	56	2.71
L dorsolateral prefrontal cortex	−38	50	20	2.67
R inferior frontal gyrus	52	12	20	3.06
L inferior frontal gyrus	−48	12	22	2.48
R premotor cortex (frontal eyefields BA8R, BA6R)	20	−4	70	3.63
L premotor cortex (frontal eyefields BA8L, BAL)	−28	−26	70	4.22
R anterior intraparietal sulcus	−50	−44	50	4.23
L anterior intraparietal sulcus	40	−48	50	3.63
R parietal occipital junction (superior parietal lobe/lateral occipital lobe)	36	−58	40	3.72
L parietal occipital junction (superior parietal lobe/lateral occipital lobe)	−32	−60	40	4.30

Activation during oddball detection as a function of parametrically increasing interval length BOLD activation cluster-corrected at z = 2.3, p = 0.05. Coordinates are given in MNI space.

Table A2. Complete list of brain regions showing significant BOLD activation during target detection as a function of parametrically increasing interval length. during odd 3 as compared to odd 1.

Table A3

Brain region	X	Y	Z	Max z
R thalamus	8	−26	0	2.89
L thalamus	−6	−26	4	3.25
R supplementary motor area	6	8	64	3.95
L supplementary motor area	−8	6	64	3.18
R dorsal ACC	2	18	26	2.39
L dorsal ACC	−8	34	24	3.21
Precunus	14	−64	46	2.82
L somatosensory cortex	−46	−32	46	3.56
R lateral occipital cortex	40	−64	44	3.59
L lateral occipital cortex	−38	−64	52	3.56

Local maxima of activation of all significant clusters (at z = 2.3, p = 0.05, cluster-corrected) varying with aware errors and with the interval effect on target detection. All coordinates are given in MNI space.

Table A3. Spatial overlap map of clusters of activation that survived, within each participant's native space, both the threshold for the awareness contrast and the threshold for parametric TTI effects during target detection.

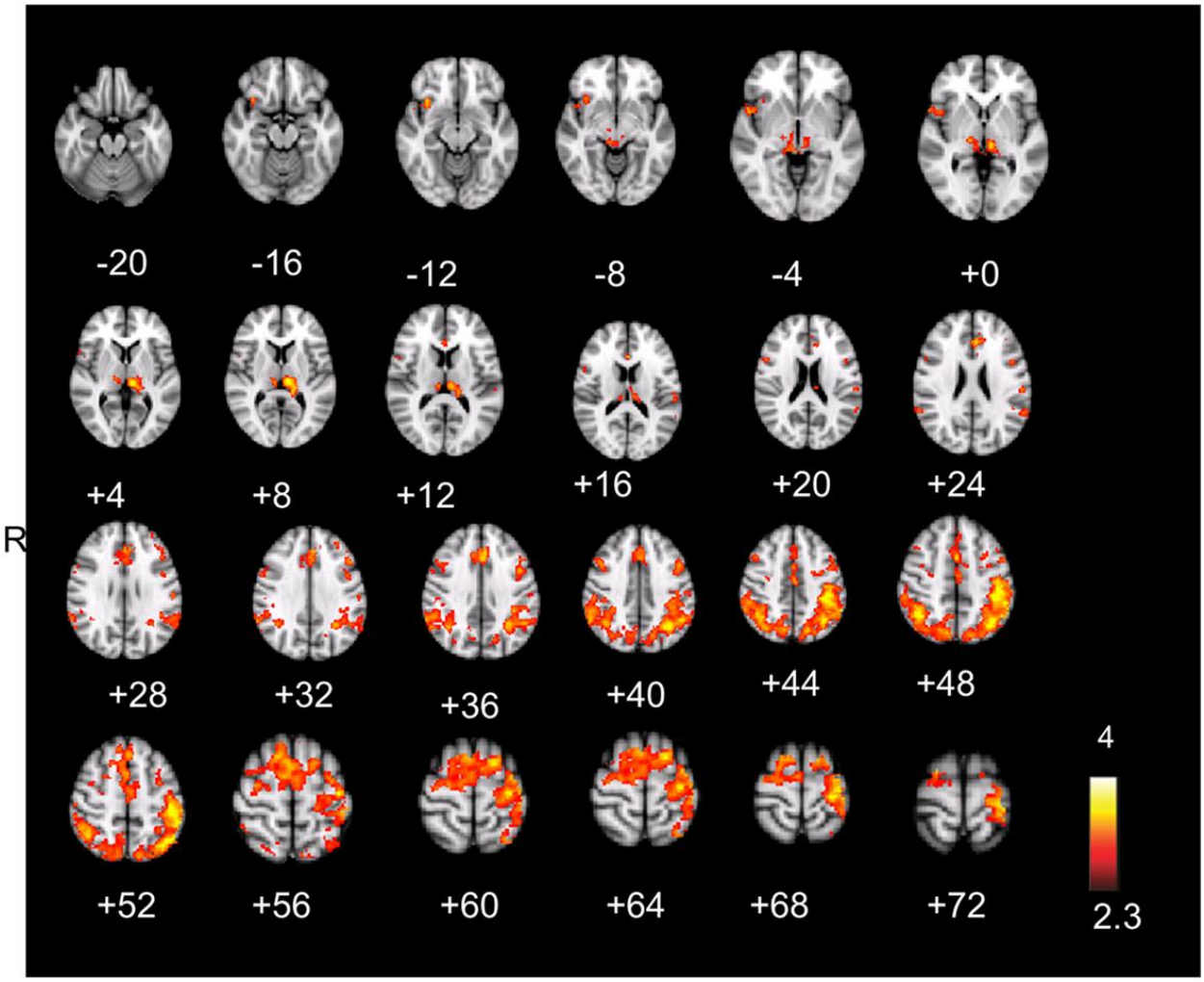

Figure A1. Neural activation on aware errors. Statistical parametrical map of difference in BOLD activation between aware and unaware errors. Red and yellow voxels represent clusters of significant BOLD signal increase across all subjects. For a full list of activated regions ($z > 2.3$, whole-brain cluster-corrected, $p < 0.05$), see Table A1.

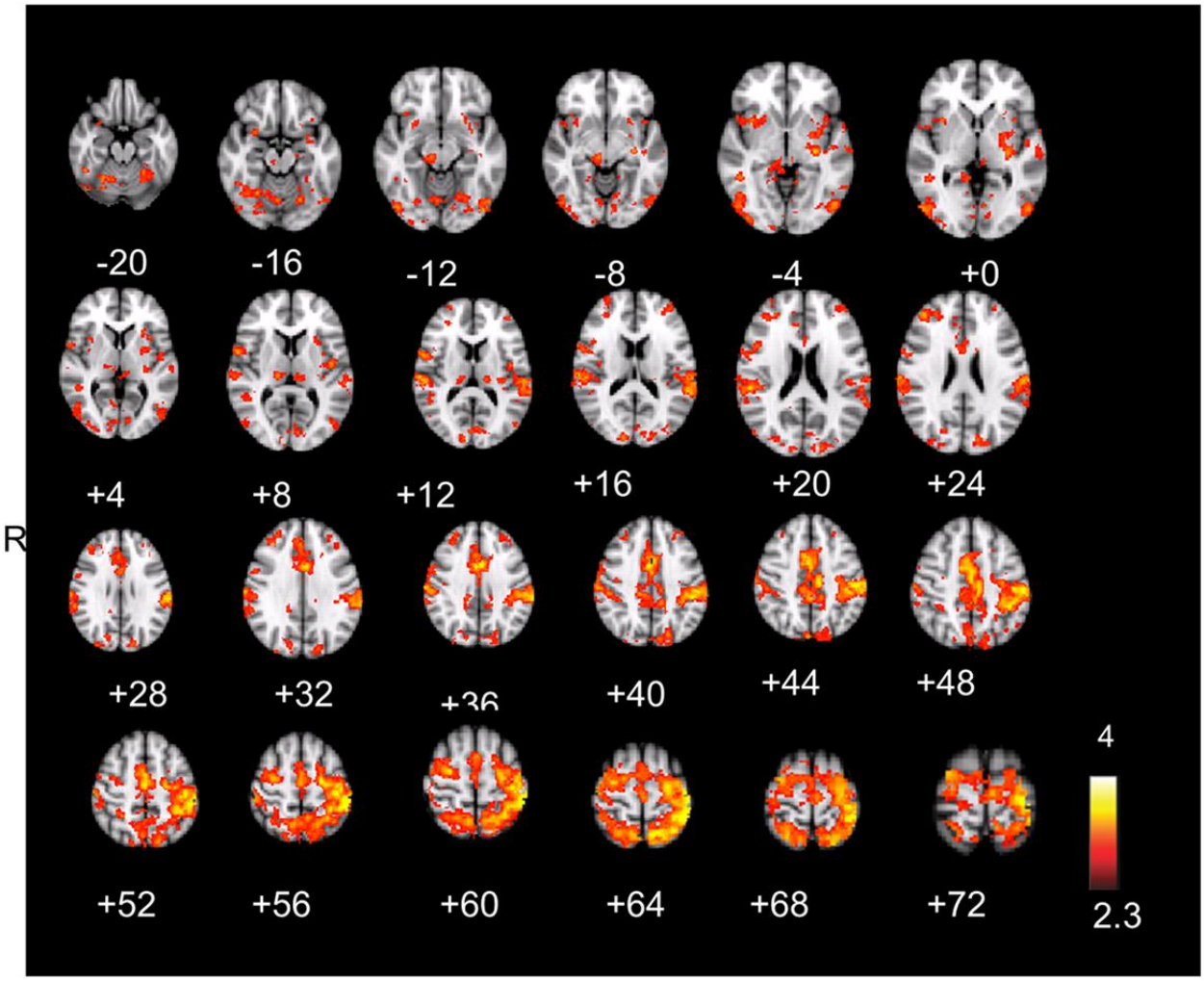

Figure A2. Illustration of brain areas showing increasing amplitude of the hemodynamic response to target stimuli with longer target interval. Target interval effects were found in numerous brain structures, including bilateral thalamus, bilateral anterior insula, dorsal anterior cingulate, supplementary motor area, dorsolateral prefrontal cortex, bilateral middle temporal gyri, bilateral pre- and postcentral gyri (somatosensory cortex), bilateral inferior and superior parietal lobules, parietal occipital junction, superior/middle and inferior frontal gyrus, precuneus, and bilateral cerebellum. The legend shows z-score value associated with the color map. The statistical parametric map has a threshold of $z > 2.6$; $p < 0.05$ (cluster-corrected). For a full list of activated regions, see Table A2.

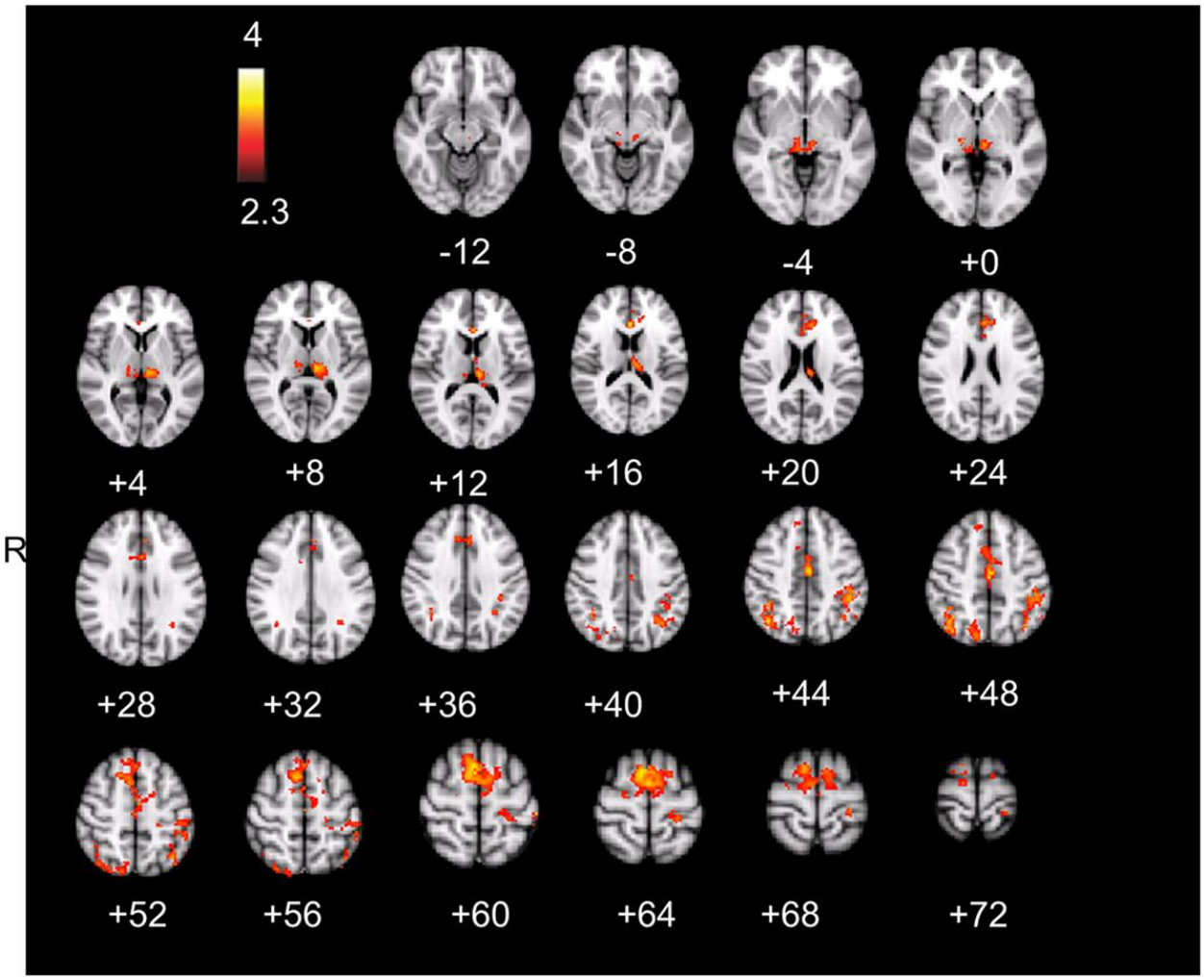

Figure A3. Statistical parametrical map of hemodynamic response varying in each individual with aware errors and with the interval effect on target detection. Red and yellow voxels represent clusters of significant BOLD signal which passed the thresholding in the target interval contrast (ITI3–ITI1) and also survived thresholding in the awareness contrast (aware versus unaware errors). Four major brain areas were involved in both contrasts: bilateral thalamus, supplementary motor area, rostral cingulate, and in bilateral parietal lobule. Furthermore, overlapping activations were found in the precuneus and lateral occipital gyrus.

Appendix Chapter 7

Supplementary Table 1. Brain regions showing significant BOLD activation during aware errors as compared to unaware errors

Aware errors>unaware errors, BOLD activation cluster corrected at z= 2.3, p= .001				
Brain region	X	Y	Z	Max z
R Anterior insula cortex	34	18	-12	3.65
R Mid insula cortex	50	8	-4	3.63
R Postcentral gyrus (somatosensory cortex BA2R)	54	-26	44	3.04
L Postcentral gyrus (somatosensory cortex BA2L, BA1L, BA3bL)	-46	-28	50	4.86
R Thalamus	10	-24	10	3.15
L Thalamus	-8	-22	8	4.39
R Brain stem	8	-30	-8	3.21
R Rostral anterior cingulate cortex	2	26	16	3.18
L Rostral anterior cingulate cortex	-2	26	16	3.18
R Dorsal anterior cingulate cortex	4	20	36	3.03
L Dorsal anterior cingulate cortex	-4	32	32	3.64
R Supplementary motor cortex (BA6R)	6	8	56	3.63
L Supplementary motor cortex (BA6L)	-6	6	60	3.04
R Precuneus cortex	4	-68	42	3.08
R Inferior frontal gyrus	52	12	20	3.06
L Inferior frontal gyrus	-48	12	22	2.48
R Premotor cortex (frontal eyefields BA8R, BA6R)	20	-4	70	3.63
L Premotor cortex (frontal eyefields BA8L, BAL)	-28	-26	70	4.22
R Anterior intraparietal sulcus	-50	-44	50	4.23

L Anterior intraparietal sulcus	40	-48	50	3.63
R Parietal occipital junction (superior parietal lobe/lateral occipital lobe)	36	-58	40	3.72
L Parietal occipital junction (superior parietal lobe/lateral occipital lobe)	-32	-60	40	4.30

Coordinates are given in MNI space.

Supplementary Table 2. Brain regions showing significant functional connectivity with anterior insula cortex during aware errors

Aware errors> unaware errors, functional connectivity of AIC				
cluster corrected at z= 2.3, p= .0.5				
Brain region	X	Y	Z	Max z
R Postcentral gyrus (primary somatosensory cortex BA2R, BA1R)	56	-22	44	2.66
L Postcentral gyrus (primary somatosensory cortex BA2R, BA1R, BA3bL)	-46	-34	56	3.54
R Anterior intraparietal sulcus	50	-38	36	2.99
L Anterior intraparietal sulcus	-40	-40	30	3.62

Coordinates are given in MNI space